EXTREME TEMPERATURE AND HEAT FLUX EVENTS IN A WEAKLY TURBULENT FLOW

Xue Chen
Department of Mechanics and
Aerospace Engineering,
Southern University of Science and
Technology,
Shenzhen, 518055, China
chenx3@sustech.edu.cn

Jiahui Han
Department of Mechanics and
Aerospace Engineering,
Southern University of Science and
Technology,
Shenzhen, 518055, China
12331116@mail.sustech.edu.cn

Minping Wan
Department of Mechanics and Aerospace Engineering,
Southern University of Science and Technology,
Shenzhen, 518055, China
wanmp@sustech.edu.cn

ABSTRACT

This study conducted spatiotemporal conditional average analyses on the extreme wall shear stress events and extreme heat flux events induced by the associated large-scale structures in the temperature field to reveal their evolution, formation mechanics and connection to the hairpin vortices. Strong local temperature fluctuations and wall-normal heat flux are generated simultaneously with the high- and low-speed large-scale structures and the accompanied rare negative and extreme positive wall shear stress. These coherent structures exhibit similar lifespans in both the velocity and temperature fields, causing significant near-wall deviations of velocity and temperature from their mean profile, and convect large regions of strong positive and negative streamwise and wall-normal heat flux downstream, significantly enhancing local turbulent heat transfer in which the wall-normal heat flux can achieve ten times higher than its temporal mean in the near-wall region.

Observations suggest that the hairpin packets near the wall envelope regions of intensified streamwise heat flux as part of the formation process of the large-scale motions and extreme events. Along the outline of the packets, the successive strong spanwise rotations at the heads of the hairpin vortices induce intense local wall-normal heat flux that lead to abrupt jump of temperature across the inclined shear layer.

INTRODUCTION

Over the past decade, the wall turbulence community has recognised that the formation mechanism and evolution dynamics of the near-wall extreme events play significant roles in surface friction drag and heat transfer. In the wall proximity, occasional negative wall-shear stress and extreme positive wall shear stress events which manifest as the prolonged tails of the probability density functions (PDF) of the wall shear stress, τ_w, drive remarkably intensified local fluctuations in skin friction and heat transfer coefficients that can reach multiple times their mean values, challenging reliable predictions of surface fatigue and thermal damage under such extreme conditions.

The dynamics of these extreme events in the velocity and vorticity fields including their role in near-wall momentum transfer, and their links to large-scale motions (LSMs) have been well studied in fully-developed wall-bounded flows (Lenaers *et al.*, 2012; Vinuesa *et al.*, 2017; Cardesa *et al.*, 2019; Guerrero *et al.*, 2020, 2022; Chen *et al.*, 2024). The negative part and the skewed positive tails of the PDF of wall shear stress correspond to two types of extreme wall shear stress events in which the negative wall shear stress events are often referred as backflow events, namely accompanied with short appearance local flow reversal on the wall, mostly confined within the viscous sublayer. Strong spanwise rotations at the heads of hairpin vortices sweep high-speed fluids toward the wall; when these fluids interact with low-speed structures formed by Q2 ejections between hairpin legs (Adrian *et al.*, 2000), they sporadically generate negative wall shear stress, accompanied with the short appearance of local backflow.

Extreme wall shear stress events involve multiphysical phenomena. The spatiotemporal analyses by Guerrero *et al.* (2022) and Chen *et al.* (2023) conducted in turbulent pipe flows showed that large-scale structures and the accompanied extreme wall shear stress events induce strong local perturbations in the pressure field, causing large regions of local adverse pressure gradients extending up to the whole boundary layer. Meanwhile, Zhang *et al.* (2023) also highlighted the role of extreme wall shear stress events in wall heat flux, demonstrating significant alterations in surface heat transfer coefficients during these events in compressible turbulent boundary layers. Given the strong correlation between the temperature field and streamwise velocity, the spatiotemporal dynamics of temperature fluctuations linked to near-wall extreme events are particularly relevant to understanding turbulent heat transfer mechanisms. However, research on the dynamics of turbulent heat transfer relative to extreme wall shear stress events remains limited. Thus, the present study performs spatiotemporal analyses of the passive scalar temperature field in both fully

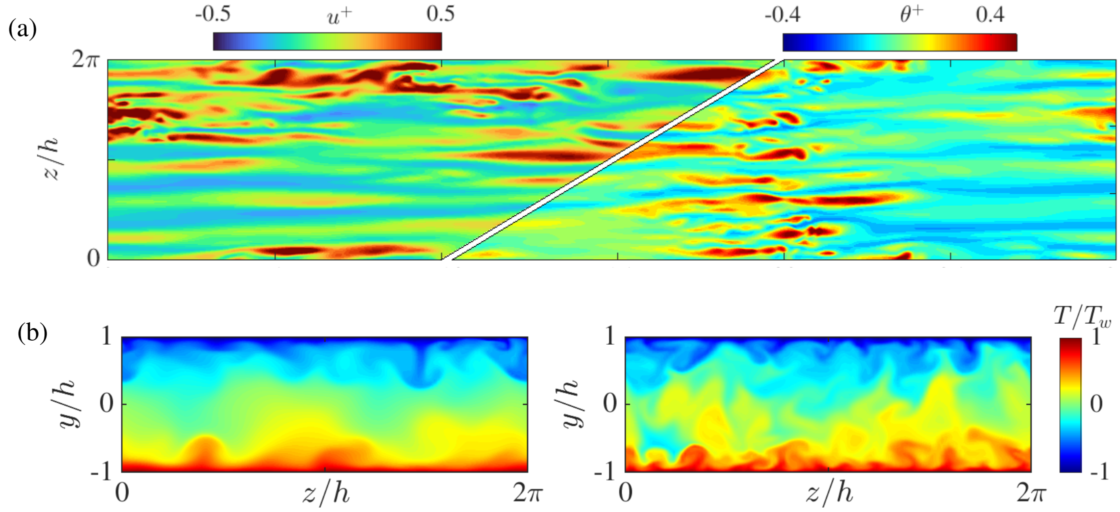

Figure 1. (a) Wall-parallel contours of streamwise velocity (left) and temperature fluctuations (right), u and θ of the weakly-turbulent flow. (b) Cross-stream contour of instantaneous temperature of the weakly turbulent flow (left) compared with fully-developed flow (right) at comparable Reynolds number.

turbulent and transitional channel flows, focused on extreme wall shear stress events. The goal is to evaluate the dynamics of associated large-scale motions in the temperature field and the resulting extreme heat flux events that accompany extreme wall friction.

METHODOLOGY

This study employed the direct numerical simulation (DNS) data of a weakly-turbulent flow in the channel at friction Reynolds number of $Re_\tau \approx 180$. The weakly turbulent flow was obtained by a similar numerical procedure as demonstrated by Chen *et al.* (2024) via simulating a viscoplastic non-Newtonian fluid with variable viscosity modelled by the power-law, $\mu = K\dot{\gamma}^{n-1}$ at a highly shear-thinning index of $n = 0.5$ where constant K relates to fluid property and $\dot{\gamma}$ is the local shear rate. This flow remained a transitional state with the mean turbulence intensity acts as a function of wall distance, showing resemblance to traditional transitional flow with turbulent spots and auto-regeneration of hairpin vortices in clusters.

The non-dimensional incompressible Navier-Stokes equations were solved in Nek5000 over a domain of $(30 \times 2 \times 2\pi)h$ (h is the channel half-height) in the streamwise, wall-normal and spanwise directions, denoted as x, y and z, respectively. The corresponding velocity fluctuations are denoted as u, v and w, and the fluctuation of temperature, T, is denoted as θ. The temperature field were solved by the passive scalar transport equation with resolved grid resolution for Batchelor scale at the given Prandtl number of $Pr = 0.71$. Periodic boundary conditions in the x and z directions were applied in both the velocity and temperature fields, and uniform wall temperature of $T_w = \pm 1$ was applied at the no-slip walls. The thermal diffusivity, $\alpha = k/(\rho C_p)$ had ρC_p set to unity.

The flow is compared with the conventional fully-developed channel flow of Newtonian fluid at comparable Reynolds number with data from Chen *et al.* (2023). The instantaneous flow structures in the weakly turbulent shear-thinning flow differ from the fully-developed flow remarkably. Figure 1 provides a visual comparison of the instantaneous velocity and temperature fields between the two flow cases. As shown by the near-wall streaks in Figure 1(a), the temperature fluctuations exhibited notably widened streaks in the turbulent spots similar to the velocity fields owing to the suppression of turbulent intensity. In Figure 1(b), the cross-stream contour of temperature shows that for the weakly turbulent flow, temperature fluctuations in regions with local laminarization are very quiescent where plume structures only appear in the turbulent regions. Meanwhile, despite the significant difference in the instantaneous fields, the near-wall mean flow statistics of the weakly turbulent flow is comparable to the fully-developed case when controlled with the same designated frictional Reynolds number in which the largely laminarized regions outside the turbulent spots have negligible influence on the mean thermal conductivity, $\bar{k}$, and wall heat flux $\overline{q_w}$.

RESULTS AND DISCUSSION

Propagation of large-scale streamwise and wall-normal heat flux structures

In this study, the negative and the extremely positive wall shear stress events are referred to the BF (backflow) events and EP events, respectively, and are defined by thresholds of $\tau_w^+ < 0$ and $\tau_w^+ > \tau^*$ where $\tau_w^* = 3.1$ following Guerrero *et al.* (2020). Spatiotemporal conditional averaging is applied around the BF and EP events separately, similar to the approach in Guerrero *et al.* (2022) and Chen *et al.* (2023). The conditionally averaged fields are denoted by $\langle\cdot\rangle$ where the distance and interval from the sampling events are represented by Δx_i and Δt, respectively.

The contours of wall shear stress and wall heat flux in Figure 2 show the temporal evolution and streamwise convection of the strong positive and negative regions of wall shear stress and wall heat flux fluctuations, τ_w' and q_w', induced by the high- and low-momentum large-scale structures. The wall shear stress and wall heat flux exhibit significant local fluctuations underneath the LSMs which yield similar patterns of strongly positive and negative τ_w' and q_w' on the wall as the LSMs propagate downstream. Figures. 2(e,f) show the time history of the profiles of $\langle\tau_w'\rangle$ and $\langle q_w'\rangle$ in the streamwise direction at $\Delta z = 0$ where q_w' is applied with an adjusted Reynolds-Colburn analogy with an additional constant term to eliminate the mismatch due to flow laminarization. Although not shown

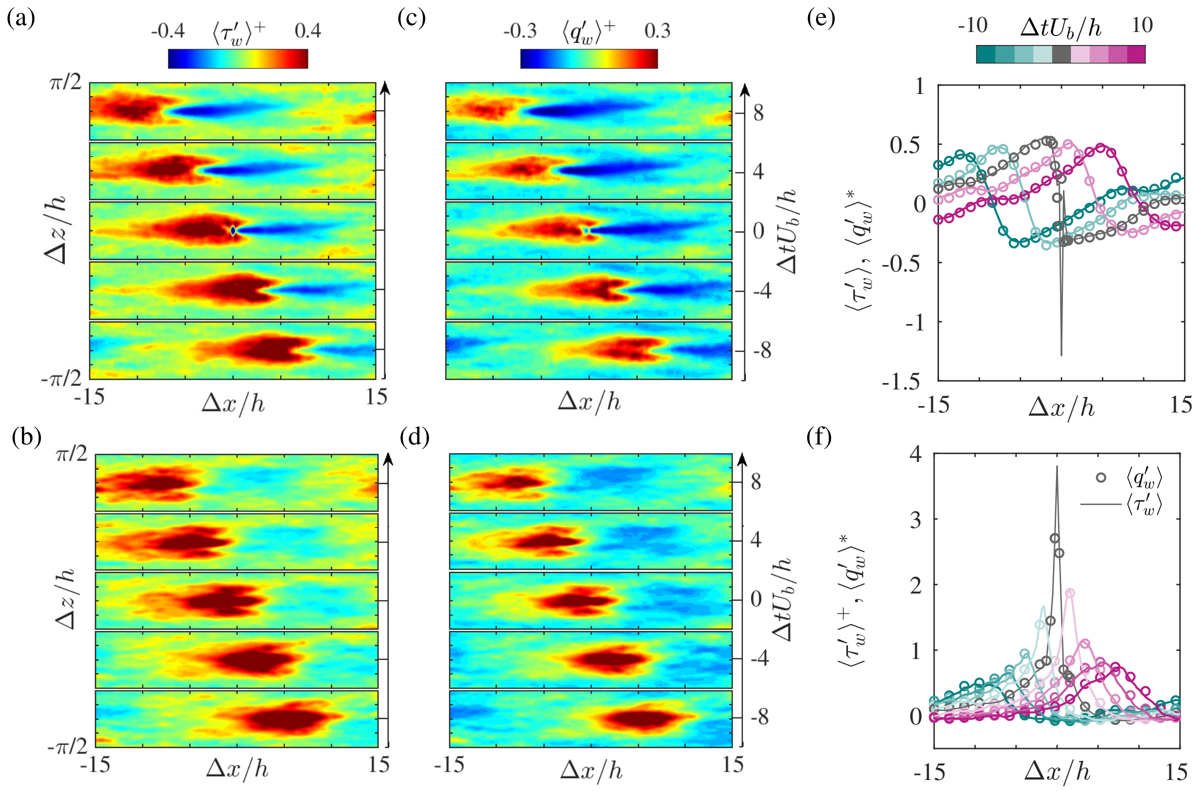

Figure 2. Contours of (a,b) the wall-shear stress fluctuation, τ'_w and (c,d) the wall heat flux fluctuation, q'_w in the spatiotemporal conditional average fields around (a,c,e) BF events and (b,d,f) EP events in the weakly turbulent flow. (e,f) The streamwise profiles of $\langle\tau'_w\rangle$ (lines) and $\langle q'_w\rangle$ (symbols) at $\Delta z = 0$ where $\langle q'_w\rangle^*$ is rescaled as $(Pr^{-2/3}U_c/U_b)\langle q'_w\rangle^+ + 0.1$.

for brevity, the streamwise profiles of $\langle\tau'_w\rangle$ and $\langle q'_w\rangle$ during the extreme events in the fully developed flow are qualitatively similar with the results in Figure 2, in which the spatial extent of the large-scale structures exhibits reduction in scale in the fully-developed flow with higher magnitudes of the wall shear stress and wall heat flux peaks.

In Figures 2(a,c), the large regions of intense wall shear stress and wall heat flux fluctuations associated with the BF events convect downstream steadily with the bulk flow, corresponding to the propagating wave of large-scale positive and negative fluctuations of wall shear stress and wall heat flux in the streamwise direction shown in Figures 2(e). The profile is rather consistent in magnitude and shape before and after the backflow event takes place during which abrupt local fluctuations of $\langle\tau'_w\rangle$ and $\langle q'_w\rangle$ are found at the critical point of zero wall shear stress under the backflow region. As illustrated in Figure 2, the strong positive and negative wall shear stress and wall heat flux regions persist for over ten large-eddy turnover times around the BF events as the associated LSMs maintain their strength while propagating downstream (Guerrero *et al.*, 2022; Chen *et al.*, 2023). Similarly, in Figures 2(a,c), the EP events result in a convected region of extremely high wall shear stress which is accompanied with high wall heat flux that propagates downstream with the LSMs, leading to a growing impulse signal with sharply intensified positive wall shear stress and wall heat flux that peaks at the location of the EP events, as shown in Figure 2(f).

The conditional averaged streamwise and wall-normal heat flux, $\langle u\theta\rangle$ and $-\langle v\theta\rangle$ are examined via being depicted on the wall-parallel plane at the vicinity of the wall (at $y^+ \approx 1$) and the streamwise plane at $\Delta z = 0$ in Figure 3. Figure 3 shows the traces of the strong streamwise and wall-normal heat flux, $\langle u\theta\rangle$ and $-\langle v\theta\rangle$ induced by the high- and low-momentum large-scale structures. The conditional averaged $1D$ profile of wall heat flux are also plotted at multiple streamwise locations with the comparison with their global mean profiles. With a similar pattern exhibited by the high- and low-momentum structures associated with the BF and EP events in the conditionally averaged velocity field (Guerrero *et al.*, 2022; Chen *et al.*, 2023), the BF and EP events causes extreme local attenuation of wall heat flux in the near-wall region which propagate as part of the large-scale motions. Figures 3(a,c) show that the large regions of intense wall heat flux fluctuations associated with the BF events propagate downstream steadily which consequently results in a travelling wave of locally peaked wall heat flux in the streamwise direction that can achieve over ten times of their mean value. The strong positive and negative wall heat flux regions persist for over ten large-eddy turnover times as the LSMs maintain their strength while propagating downstream. Similarly, the EP events result in a convected region of extremely high wall shear stress and wall heat flux that propagates with the LSMs, leading to a growing impulse signal of wall shear stress and wall heat flux that peaks at the EP events.

These LSMs in the temperature field and the associated extreme wall heat flux can extend up beyond the boundary-layer thickness. As shown in Figures 3(a,b), the streamwise heat flux exhibits similar behaviour to the streamwise velocity fluctuation (Guerrero *et al.*, 2020) during the extreme events, with the high- and low-streamwise heat flux regions joining around the backflow. Meanwhile, as shown in Figure 3(b), the EP events are accompanied by a strong region of streamwise heat flux, leaving intense local surges and reductions of $\langle u\theta\rangle$ in the near-wall region. The wall-normal heat flux, $-v\theta$ also exhibits an acute response to the extreme events. In Figure 3(c), the low-speed structure adjacent to the wall induces strong

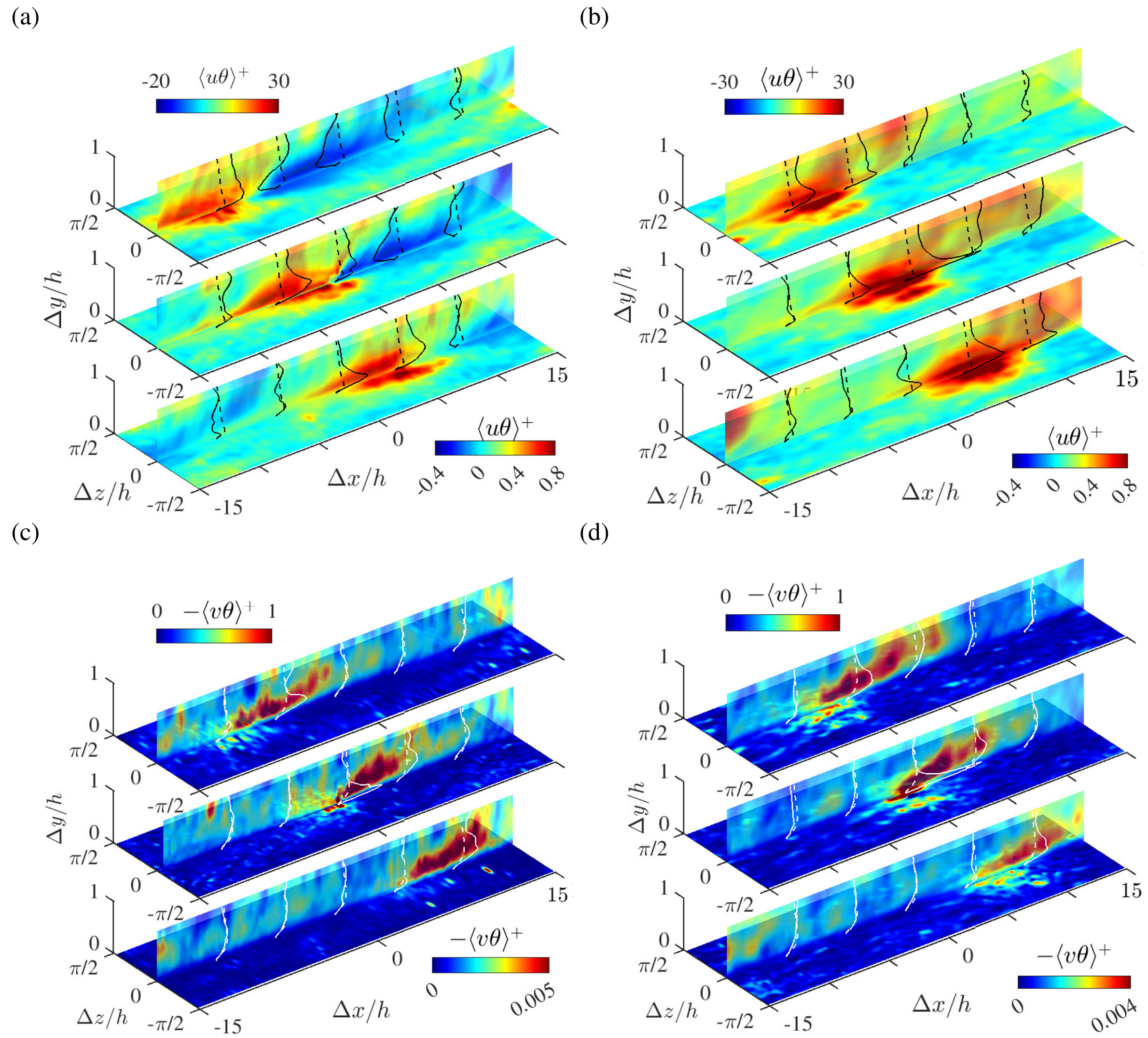

Figure 3. Wall-parallel (at $y^+ \approx 1$) and streamwise-wall-normal contours of (a,b) the streamwise heat flux and (c,d) the wall-normal heat flux in the spatiotemporal conditional average fields at $\Delta t U_b/h = -8$, 0, 8 around (a,c) BF events and (b,d) EP events. The solid and dashed lines are the local conditional average and the global mean profiles, respectively.

wall-normal heat flux in the low-momentum region. During the extreme events, the wall-normal heat flux deviates substantially from its mean value near the wall, particularly at the upstream end of the low-speed structure where backflow occurs. A similar region of strong wall-normal heat flux is observed downstream of the EP events, as shown in Figure 3(d). The pronounced near-wall surge in wall-normal heat flux caused by the EP events closely resembles the $-\langle v\theta \rangle$ structure associated with the BF events.

Formation mechanism of strong heat flux regions

The formation mechanism of the observed extremely intensified heat flux during the extreme events was then examined in the instantaneous fields for their relations with the hairpin vortices. In Figure 4, two distinct hairpin packets are labelled as A and B with ascending numbering from the older and more elevated hairpins to the upstream younger and finer ones nearer the wall. The contours are plotted at the spanwise location that is approximately at the centre of the two packets, catching the hairpin heads which are depicted by the enclosed contours of Q on the contour. The larger packet A is associated with backflow at the upstream end of the packet, at the tail-tip of strong low-speed structure induced by the outward counter-rotating quasi-streamwise vortices, i.e., the aligned legs of the hairpins vortices. In Figure 4(a), the upper edge of the strong streamwise heat flux region forms a thin layer of prominent wall-normal temperature gradient, which align with the undulating outline of the hairpin packets. Such observation also applies to packet B which is not strong enough to cause near-wall flow reversal, though generating large regions of strong positive streamwise heat flux within the packet.

Figure 4(b) shows the contour of the wall-normal heat flux. The strong spanwise rotations at the heads of the hairpin structures are responsible for the enhanced wall-normal heat flux along the heads and within the packet. The strong spanwise vortices induce strong local wall-normal heat flux events under an analogous mechanism to the engulfment of the turbulent non-turbulent interface or the internal shear layers, enhancing the local thermal mixing.

Consistent with the observations by Chen *et al.* (2024), the strong spanwise rotations at the heads of the hairpin structures are responsible for the enhanced wall-normal heat flux along the heads and within the packet. The strong spanwise vortices induce strong local wall-normal heat flux events un-

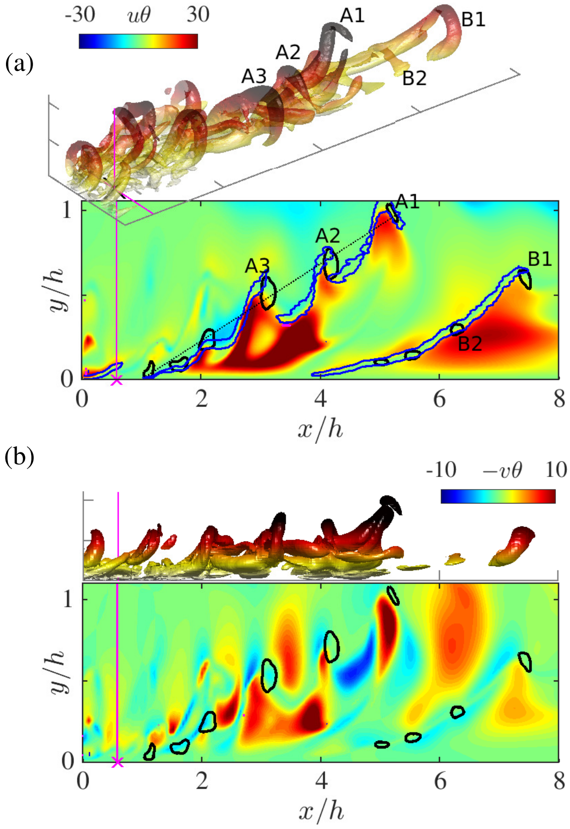

Figure 4. Isosurface of $Q = 0.1$ coloured by wall-normal elevation and the aligned contours of (a) $u\theta$ and (b) $-v\theta$ in an instantaneous snapshot. The backflow region is marked by '×'. The heads of the hairpin vortices are indicated by the labelled contour of Q. The blue lines in (a) are the contours of $\partial\theta^+/\partial y^+ \approx 0.3$.

der an analogous mechanism to the engulfment of the turbulent non-turbulent interface or the internal shear layers, enhancing the local thermal mixing.

CONCLUSION

Spatiotemporal analyses were conducted in a weakly turbulent channel flow at a low Reynolds number with passive scalar temperature field. Results from the conditionally averaged fields reveal that extreme wall friction events and their associated large-scale motions (LSMs) play a vital role in turbulent heat transfer. The extreme fluctuations of wall shear stress are accompanied with correlated extreme wall heat flux fluctuations. As the large-scale motions and the correlated large-scale temperature structures convected downstream in both the velocity and temperature fields, the high- and low-speed fluids induce extreme local fluctuations of velocity, temperature and heat flux in both streamwise and wall-normal direction, with the peak heat flux exceeding the mean value by nearly an order of magnitude on average in the near-wall region.

With similar mechanism of the near-wall momentum transfer, the hairpin vortices have a key role in the wall-normal transport of heat as they coherently elevate the temperature isosurface. Observations from the instantaneous fields suggest that the hairpin packets would envelop a prominent region of enhanced turbulent heat transfer, and are responsible for the exceedingly strong heat flux events.

REFERENCES

Adrian, R., Meinhart, C. & Tompkins, C. D. 2000 Vortex organisation in the outer region of the turbulent boundary layer. *Journal of Fluid Mechanics* **422**, 1–54.

Cardesa, J. I., Monty, J. P., Soria, J. & Chong, M. S. 2019 The structure and dynamics of backflow in turbulent channels. *Journal of Fluid Mechanics* **880**, R3.

Chen, X., Chung, Y. M. & Wan, M. 2023 Backflow structures in turbulent pipe flows at low to moderate Reynolds numbers. *Journal of Fluid Mechanics* **966**, A38.

Chen, X., Chung, Y. M. & Wan, M. 2024 The statistical characteristics and auto-regeneration of backflow in non-Newtonian turbulent pipe flow. *Physics of Fluids* **36**, 025121.

Guerrero, B., Lambert, M. F. & Chin, R. C. 2020 Extreme wall shear stress events in turbulent pipe flows: spatial characteristics of coherent motions. *Journal of Fluid Mechanics* **904**, A18.

Guerrero, B., Lambert, M. F. & Chin, R. C. 2022 Precursors of backflow events and their relationship with the near-wall self-sustaining process. *Journal of Fluid Mechanics* **933**, A33.

Lenaers, P., Li, Q., Brethouwer, G., Schlatter, P. & Örlü, R. 2012 Rare backflow and extreme wall-normal velocity fluctuations in near-wall turbulence. *Physics of Fluids* **24** (3), 035110.

Vinuesa, R., Örlü, R. & Schlatter, P. 2017 Characterisation of backflow events over a wing section. *Journal of Turbulence* **18** (2), 170–185.

Zhang, P., Wan, J., Dong, S., Liu, N., Sun, D. & Lu, X. 2023 Conditional analysis on extreme wall shear stress and heat flux events in compressible turbulent boundary layers. *Journal of Fluid Mechanics* **974**, A38.